**Supplementary Materials**

# Spin Vector Control for Heisenberg-Inspired Probabilistic Computing

Yuanqiu Tan ‡,[1,2] Rahul Tripathi ‡, [1,2] Saleh Bunaiyan,[4,5] Ryan Wagner,[3] Neil Dilley,[2] Kerem Camsari,[4] Joerg Appenzeller,[1,2] and Zhihong Chen*[1,2]

[1]*Electrical and Computer Engineering, Purdue University, West Lafayette, Indiana, USA*

[2]*Birck Nanotechnology Center, Purdue University, West Lafayette, Indiana, USA*

[3]*Mechanical Engineering, Purdue University, West Lafayette, Indiana, USA*

[4]*Electrical and Computer Engineering, University of California, Santa Barbara, California, USA*

[5]*Engineering Department, King Fahd University of Petroleum & Minerals (KFUPM), Dhahran 31261, Saudi Arabia*

**To whom correspondence should be addressed.*

*E-mail:* zhchen@purdue.edu

Table of Contents

**1. Reciprocal spin transport characteristics of non-local lateral graphene spin valves** ..... 3

**2. The spatial dependence of the electrochemical potential μ for spin-up and spin-down electrons in the graphene non-local spin valve configuration** ..... 4

**3. Spin transport of dual spin injection between 45°/135° through non-local lateral graphene spin valve** ..... 5

**4. HSPICE Simulation** ..... 6

**5. Spin transport of dual spin injection between 15°/165° through non-local lateral graphene spin** ..... 10

## 1. Reciprocal spin transport characteristics of non-local lateral graphene spin valves

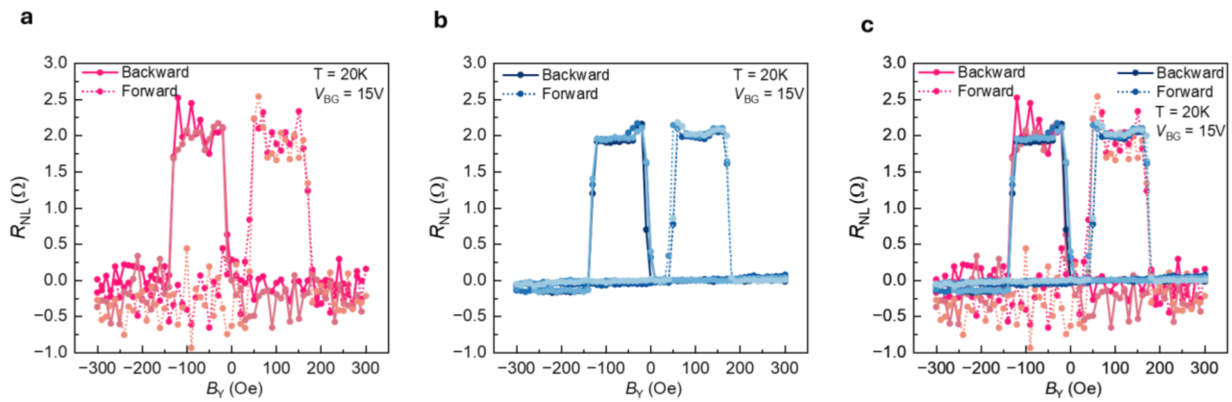


**Fig. S1. Reciprocal readout with opposite spin injection polarity. a,** Three repeated non-local spin valve measurements with spin injection through FM electrode 3 and detection at electrode 2, as schematically illustrated in Fig. 1a; **b**, Three repeated non-local spin valve measurements with spin injection through FM electrode 2 and detection at electrode 3; **c**, Combined plot of all measurements from **a** and **b**, demonstrating signal robustness, reproducibility, and Onsager reciprocal relations.

## 2. The spatial dependence of the electrochemical potential μ for spin-up and spin-down electrons in the graphene non-local spin valve configuration

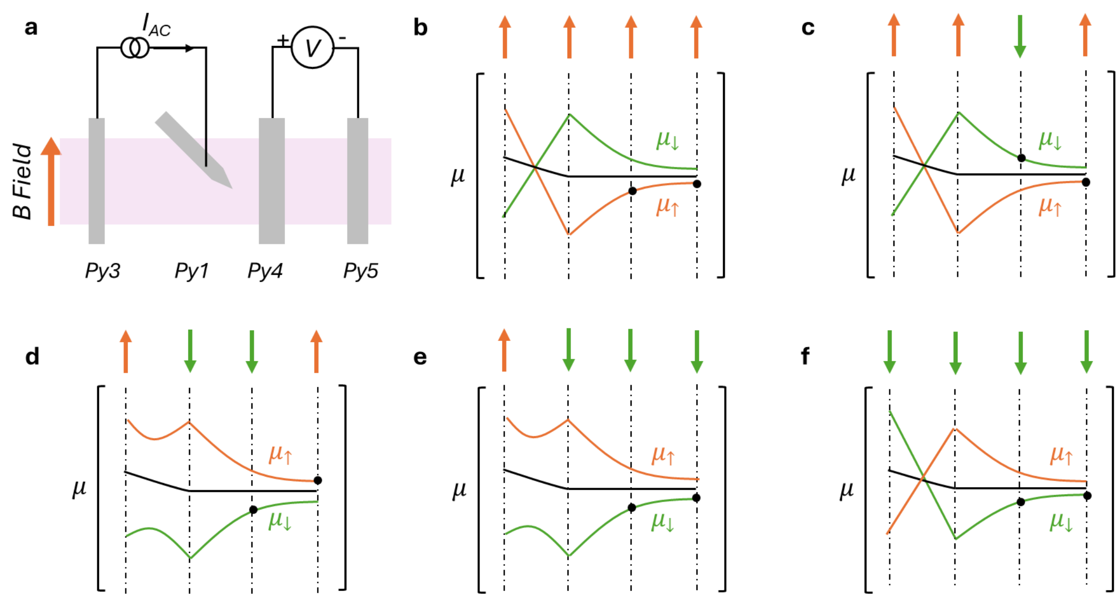


**Fig. S2. Spatial evolution of electrochemical potentials in the graphene non-local spin valve. a**, Schematic of a monolayer graphene lateral NLSV device. **b-f**, The spatial profiles of the electrochemical potentials for spin-up and spin-down electrons corresponding to sequential magnetization configurations during a magnetic-field sweep from positive to negative field under single-injection conditions. Each configuration change produces a distinct resistance step in the non-local signal. The potential difference between panels **b** and **c** corresponds to the first resistance jump labeled in Fig. 2c, while the transition from **c** to **d** corresponds to the second jump, and so forth.

For dual-injection configurations, additional resistance steps arise depending on the relative injection conditions of $I_{\mathrm{Py1}}$ and $I_{\mathrm{Py2}}$. As illustrated in Fig. 3, magnetization reversal of Py1 and Py2 introduces extra changes in the electrochemical potential profiles, resulting in an additional resistance step between panels **d** and **e** compared to the single-injection case. For example, with a relatively balanced injection from Py1 and Py2 (Fig. 3a), the electrochemical potential associated with Py1 has already transitioned to configuration **d**, while the potential associated with Py2 remains in configuration **c** due to its different switching field. This intermediate configuration produces an additional resistance step in the non-local signal. These spatial electrochemical potential traces provide a microscopic interpretation of the stepwise evolution observed in the non-local spin valve signals under different magnetic-field conditions.

### 3. Spin transport of dual spin injection between 45°/135° through non-local lateral graphene spin valve

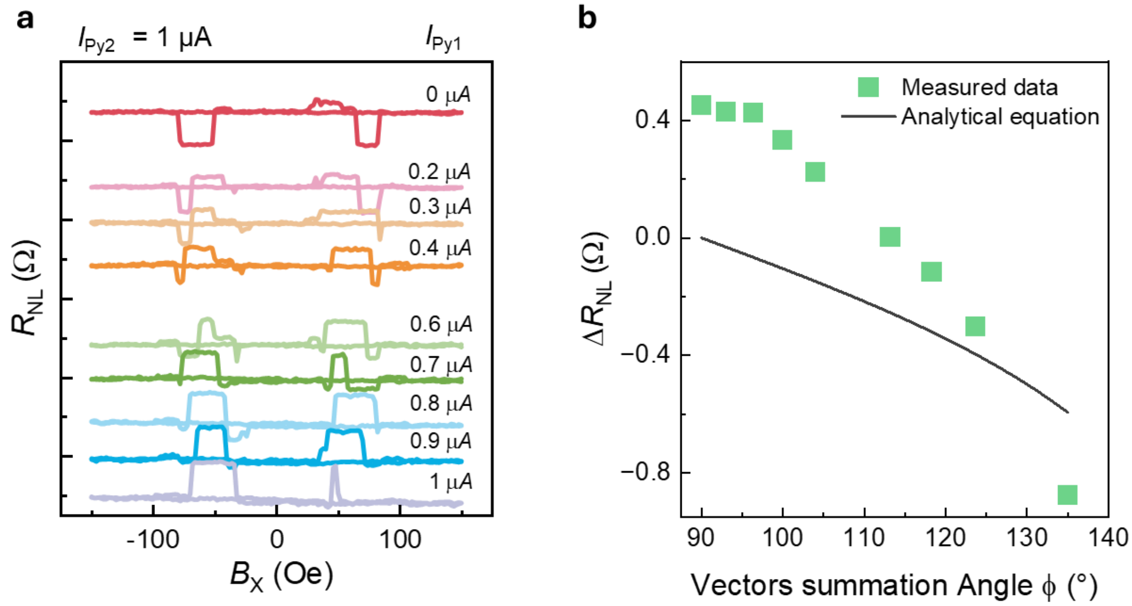


**Fig. S3. Non-colinear spin vector readout by graphene non-local spin valve. a**, Non-local spin valve signals obtained by varying $I_{Py1}$ while keeping $I_{Py2}$ = 1 μA. **b**, Corresponding $\Delta R_{NL}$ (squares) as a function of the angle $\emptyset$, with modulation achieved by changing the current injected into Py1 while holding Py2 current constant. All spin transport measurements are conducted with T = 20 K and $V_{BG}$ = 15 V.

Starting from the single injection from Py2, the resultant $\Delta R_{NL}$ presents negative values. As the current injected from Py1 is increased, the resultant spin vector rotates and $\Delta R_{NL}$ shows less negative and eventually turning positive. The non-local spin valve scan with B-field under $I_{Py1} = I_{Py2}$ = 1 μA exhibit the same switching sequence observed in Fig. 4.

## 4. HSPICE Simulation

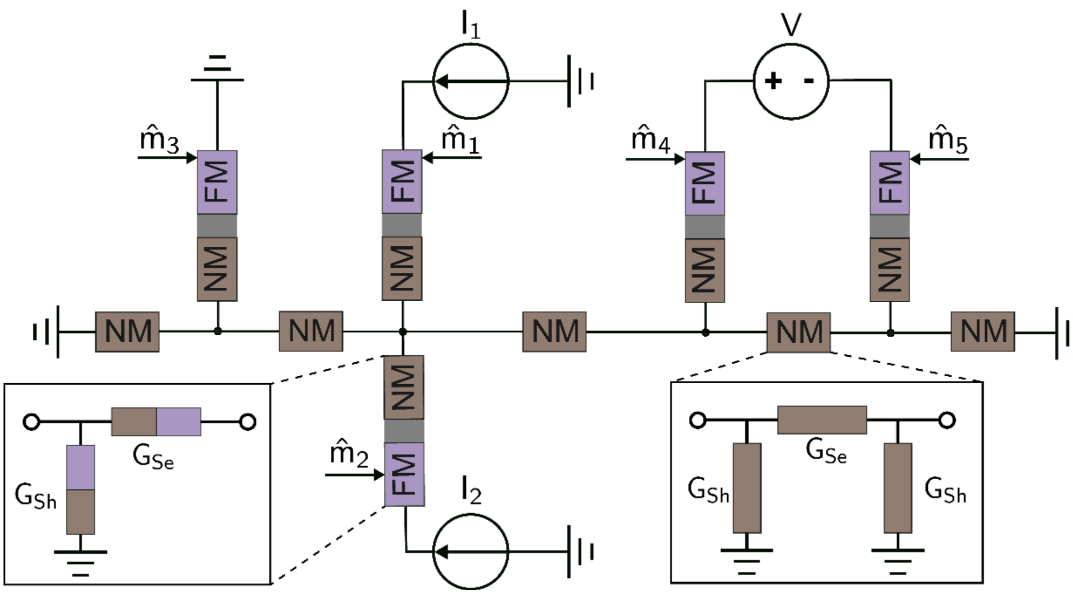


**Fig. S4. Simulated non-local spin valve using spin-circuit.** The device transport is captured by two modules: the Non-Magnet (NM) and the Ferromagnet and non-magnet interface (FM|NM). The NM module represents the graphene channels while, the FM|NM modules represent the interface between graphene and the Permalloy (Py) ferromagnet. All circuit components are described by four components: charge and spins in the $(x, y, z)$ directions. The injected spin current in the channel is controlled by $I_1$ and $I_2$, where the two injecting magnets $(\hat{m}_1, \hat{m}_2)$ are oriented along 45° and 135°, respectively. The measured non-local resistance $R_{NL}$ is described by the ratio between the non-local voltage (V) and the total injected charge current ($I_1 + I_2$).

In this section, we describe the spin-circuit approach used to emulate the non-local spin-valve device shown in Fig. 2 of the main manuscript. This modeling approach was employed to obtain both the numerical and analytical results reported in Fig. 4-5 and Fig S3.

The spin-circuit models are derived based on the work of Bauer, Brataas, and Kelly on magnetoelectric circuit theory[1]. These models were further extended into circuit formulations that can be readily integrated with standard circuit simulators (e.g., HSPICE)[2–5]. This spin-circuit approach generalizes conventional charge-based circuits to include spin-dependent transport, where each voltage node is represented by a four-component vector: one charge component and three spin components along the $(x, y, z)$ directions. Consequently, each conductance element is expressed as a $4 \times 4$ matrix.

**Non-magnet (NM):** The NM model consists of three $4 \times 4$ matrices: one series matrix $G_{Se}$ and two shunt matrices $G_{Sh}$, as shown in Fig. S4. The standard charge and spin transport are represented by $G_{Se}$, while the relaxation of spin transport is captured by $G_{Sh}$. These matrices are constructed as follows:

$$G_{Se} = \begin{bmatrix} G_c & 0 & 0 & 0 \\ 0 & G_s & 0 & 0 \\ 0 & 0 & G_s & 0 \\ 0 & 0 & 0 & G_s \end{bmatrix}, G_{Sh} = \begin{bmatrix} 0 & 0 & 0 & 0 \\ 0 & G_S' & 0 & 0 \\ 0 & 0 & G_S' & 0 \\ 0 & 0 & 0 & G_S' \end{bmatrix}$$

The charge conductance is given by $G_C = A_{NM}/(\rho_{NM} L_{NM})$, the series spin conductance is given by $G_s = A_{NM}/(\rho_{NM} \lambda_s) \operatorname{csch}(L_{NM}/\lambda_s)$, and the shunt spin conductance is given as $G_S' = A_{NM}/(\rho_{NM} \lambda_s) \tanh(L_{NM}/2\lambda_s)$, where $A_{NM}$ is the NM's cross-sectional area, $\rho_{NM}$ is the NM's resistivity, $\lambda_s$ is the spin-diffusion length and $L$ is the NM length.

**Ferromagnet and Non-Magnet Interface (FM|NM):** The FM|NM interface model consists of two $4 \times 4$ conductance matrices: a series conductance $G_{Se}$ and a shunt conductance $G_{Sh}$. Both matrices assume that the ferromagnet's magnetization is initially aligned along the $+z$ direction. The two conductance are constructed as follows

$$G_{Se} = G_0 \begin{bmatrix} 1 & P & 0 & 0 \\ P & 1 & 0 & 0 \\ 0 & 0 & 0 & 0 \\ 0 & 0 & 0 & 0 \end{bmatrix}, G_{Sh} = G_0 \begin{bmatrix} 0 & 0 & 0 & 0 \\ 0 & 0 & 0 & 0 \\ 0 & 0 & a & b \\ 0 & 0 & -b & a \end{bmatrix}$$

where $G_0$ is the interface conductance, $P$ is the interface polarization, and $a, b$ represent the real and imaginary parts of the spin-mixing conductance, respectively. The conductance dependence on the magnetization orientation $\hat{m}_i = (\cos\phi_i \sin\theta_i, \sin\phi_i \sin\theta_i, \cos\theta_i)$ is incorporated through the rotation $G_{\{se,sh\}} = [U_R]^T \left[G_{\{se,sh\}}\right][U_R]$, where the rotation matrix $U_R$ is given by

$$\left[\begin{array}{c|cccc} & c & z & x & y \\ \hline c & 1 & 0 & 0 & 0 \\ z & 0 & \cos\theta & \sin\theta\cos\phi & \sin\theta\sin\phi \\ x & 0 & -\sin\theta\cos\phi & \cos\theta + \sin^2\phi(1-\cos\theta) & -\sin\phi\cos\phi(1-\cos\theta) \\ y & 0 & -\sin\theta\sin\phi & \sin\phi\cos\phi(1-\cos\theta) & \cos\theta + \cos^2\phi(1-\cos\theta) \end{array}\right]$$

**Spin-Circuit Numerical Simulation**

Using the $4 \times 4$ spin-circuit approach, we construct the non-local spin-valve setup shown in Fig. 2 of the main manuscript, which consists of five ferromagnets connected through a graphene channel. The complete circuit implementation, realized in HSPICE, is illustrated in Fig. S4. The transport in the device is captured using the NM module, which represents the graphene channels, and the FM|NM interface module, which models the interface between the graphene and the Permalloy (Py) ferromagnets.

The injected spin current in the channel is controlled by the charge-current sources $I_1$ and $I_2$, which are connected to the two injecting ferromagnets with magnetization directions $\hat{m}_1$ and $\hat{m}_2$ , oriented at $45^{\circ}$ and $135^{\circ}$, respectively. The non-local resistance $R_{NL}$ is defined numerically as the ratio between the measured non-local voltage $V$ at the detector and the total injected charge current $(I_1 + I_2)$. The parameters used to generate the numerical results presented in Fig. 4 and 5 are summarized in Table S1.

Table S1 Used Parameters for spin-circuit simulation

| Parameter | Value | Unit |
|---|---|---|
| Interface polarization for detector ($P_{det}$) | 0.5 | – |
| Interface polarization for injector 1 ($P_1$) | 0.5 | – |
| Interface polarization for injector 2 ($P_2$) | 0.5 | – |
| Interface conductance ($G_0$) | 0.001 | S |
| Spin-Mixing conductance real part ($aG_0$) | 0.001 | – |
| Spin-Mixing conductance Imaginary part ($bG_0$) | 0 | – |
| NM Spin-Diffusion Length ($\lambda_s$) | 500 | nm |
| NM Resistivity ($\rho_{NM}$) | $2.35 \times 10^{-8}$ | $\mu\Omega \cdot$ cm |
| NM Length ($L_{NM}$) | 500 | nm |
| NM Area ($A_{NM}$) | $5.5 \times 10^{-16}$ | $m^2$ |

**Analytical Derivation of Non-Local Resistance**

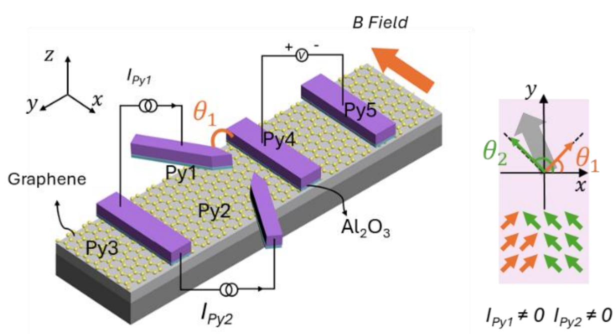


**Fig. S5. Schematic illustration of a lateral NLSV monolayer graphene device.** The dual injection electrodes are tilted to $\theta_1$ and $\theta_2$ relative to the easy-field of detector electrode in x-axis.

Building on the generalized $4 \times 4$ spin-circuit approach described above, we derive an analytical expression for the non-local resistance $R_{NL}$ using standard nodal analysis. For mathematical simplicity, we assume that each magnet has low conductance, such that the $G_0 \ll 1$ holds and the ratio between the spin-diffusion length and the channel length satisfies $\lambda_s / L_s = 1$. Under these assumptions, the approximate analytical expression for $R_{NL}$ is given by

$$R_{NL} \approx \frac{R_{ch}\, P_{det}\, (P_1 I_1 \cos\theta_1 + P_2 I_2 \cos\theta_2)}{9(I_1 + I_2)}$$

Where $R_{ch} = (\rho_{NM}\, L_{NM})/A_{NM}$ is the graphene channel resistance, $P_{det}$ is the detector polarization, $P_{1,2}$ are the polarizations of the two injectors, and $\theta_{1,2}$ denote their orientation angles with respect to the detector. In the device shown in Fig. 2, the orientation of the first injecting magnet is fixed at $\theta_1 = 45^{\circ}$ and that of the second injector at $\theta_2 = 135^{\circ}$. This analytical expression was used to obtain the results reported in Figs. 4 and 5.

## 5. Spin transport of dual spin injection between 15°/165° through non-local lateral graphene spin

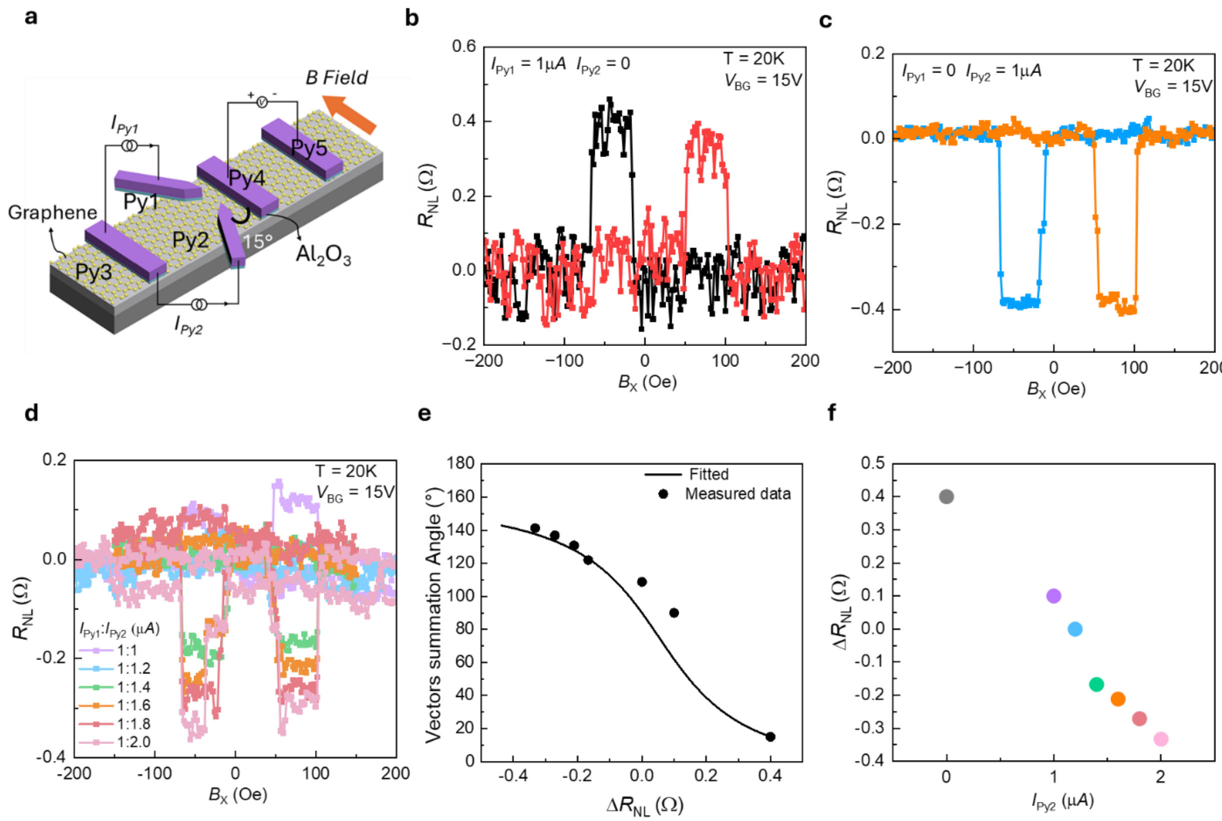


**Fig. S6. Spin vector readout by graphene non-local spin valve and theoretical modeling. a**, Schematic of lateral non-local spin valve device on monolayer graphene spin valve, with Py ferromagnetic electrodes and $Al_2O_3$ tunneling barrier; **b**, Non-local spin signal with only current injection through Py1, with T = 20 K and $V_{BG}$ = 15 V, showing nonlocal resistance of 0.4 Ω; **c**, Non-local spin signal with only current injection through Py2, showing nonlocal resistance of -0.4 Ω; **d**, Non-local spin signals with different current injections through Py2, while keeping the same current injection from Py1; **e**, Spin signal $R_{NL}$ as a function of the angle φ of the accumulated spin tuned by the dual injection. **f**, Summary of the non-local resistance with different current injections through Py2.

In this case, the ferromagnetic injector electrodes are oriented at 15° and 165° relative to the easy axis of the detector electrode. As shown in Fig. S6a, the device preserves the same graphene lateral non-local spin valve geometry as Fig. 2a. Because the injectors are positioned at 15° and 165°, the resulting spin vector exhibits a different projection onto the detector's easy axis compared to the 45° and 135° configuration, as illustrated in Fig. S6e. Nevertheless, the underlying vector summation principle remains the same: the resultant spin vector gradually transitions from a positive to a negative projection on the detector's axis as the relative injection currents vary, leading to a clear sign reversal in the non-local resistance $\Delta R_{NL}$, as shown in Fig. S6d.

Fig. S6f shows the linear relationship between $R_{NL}$ and current injected into Py2 ($I_{Py2}$), consistent with the following relations:

$$V_{NL_1} = R * I_{Py1} * \cos\Theta$$

$$V_{NL_2} = -R * I_{Py2} * \cos\Theta$$

$$V_{NL} = V_{NL_1} + V_{NL_2} = R * (I_{Py1} - I_{Py2}) \cos\Theta$$

This alternative configuration enables a distinct mode of spin vector summation and further demonstrates the robustness and tunability of our dual-injection method for manipulating spin orientations over a broader vector space.

## References


1. Brataas, A., Bauer, G. & Kelly, P. Non-collinear magnetoelectronics. *Physics Reports* **427,** 157–255 (2006).
2. Srinivasan, S., Sarkar, A., Behin-Aein, B. & Datta, S. All-spin logic device with inbuilt Nonreciprocity. *IEEE Transactions on Magnetics* **47,** 4026–4032 (2011).
3. Manipatruni, S., Nikonov, D. E. & Young, I. A. Modeling and design of Spintronic Integrated Circuits. *IEEE Transactions on Circuits and Systems I: Regular Papers* **59,** 2801–2814 (2012).
4. Camsari, K. Y., Ganguly, S. & Datta, S. Modular approach to Spintronics. *Scientific Reports* **5,** (2015).
5. Khokhriakov, D. *et al.* Multifunctional spin logic operations in graphene spin circuits. *Physical Review Applied* **18,** (2022).